Butterfly Hysteresis and Slow Relaxation of the Magnetization in $(Et_4N)_3Fe_2F_9$: Manifestations of a Single-Molecule Magnet

Ralph Schenker [a], Michael N. Leuenberger [b],

Grégory Chaboussant [a], Hans U. Güdel [a,*], and Daniel Loss [b]

[a] *Departement für Chemie und Biochemie, Universität Bern, Freiestrasse 3, CH-3000 Bern 9, Switzerland*

[b] *Departement für Physik und Astronomie, Universität Basel, Klingelbergstrasse 82, 4056 Basel, Switzerland*

Abstract

$(Et_4N)_3Fe_2F_9$ exhibits a butterfly–shaped hysteresis below 5 K when the magnetic field is parallel to the threefold axis, in accordance with a very slow magnetization relaxation in the timescale of minutes. This is attributed to an energy barrier $\Delta = 2.40$ K resulting from the $S = 5$ dimer ground state of $[Fe_2F_9]^{3-}$ and a negative axial anisotropy. The relaxation partly occurs via thermally assisted quantum tunneling. These features of a single-molecule magnet are observable at temperatures comparable to the barrier height, due to an extremely inefficient energy exchange between the spin system and the phonons. The butterfly shape of the hysteresis arises from a phonon avalanche effect.

Key words: Iron, Single-Molecule Magnet, Butterfly Hysteresis, Phonon Avalanche

PACS: 75.45.+j, 75.50.Xx, 75.50.Tt

1 Introduction

The discovery of macroscopic quantum spin tunneling and molecular magnetic hysteresis at cryogenic temperatures in the spin cluster compounds $[Mn_{12}O_{12}(OAc)_{16}(H_2O)_4] \cdot 2HOAc \cdot 4H_4O$ (**Mn_{12}**),[1–4] $[Fe_8O_2(OH)_{12}(tacn)_6]^{8+}$ (tacn = 1,4,7–triazacyclononane) (**Fe_8**),[5] and various Mn_4 clusters $[Mn_4O_3X(OAc)_3(dbm)3]$ (dmb^- = dibenzoylmethanate, X = F, Cl, Br, OAc) (**Mn_4**)[6,7] has revitalized the field of molecular magnetism. Chemists have joined forces with physicists in an attempt to fully characterize and understand the new phenomena and to develop strategies to design and prepare other members of this new family of single molecule magnets (SMMs). So far a number of further SMMs have been discovered, mostly by means of ac susceptibility, among them several manganese clusters,[8–11] as well as tetranuclear vanadium[12] and iron[13] complexes. All these compounds contain clusters with at least four paramagnetic centers.

Here we report low-temperature magnetic properties of $(Et_4N)_3Fe_2F_9$ (**Fe_2**), which clearly show effects of slow relaxation and quantum tunneling. To our knowledge the $[Fe_2F_9]^{3-}$ dimer is the smallest exchange-coupled unit so far to exhibit this type of phenomenon.

2 Experimental

$(Et_4N)_3Fe_2F_9$ was prepared as small needle-shaped crystals according to ref. [14]. The product was characterized by X-ray powder diffraction using the struc-

* Corresponding author, hans-ulrich.guedel@iac.unibe.ch, fax: +41 31 631 43 99.

tural information from ref. [15]. It crystallizes in the space group $P6_3/m$ with the trigonal axes of the $[Fe_2F_9]^{3-}$ dimers parallel to the hexagonal c axis, see the inset of Fig. 1. Due to their water sensitivity, single crystals of $\mathbf{Fe_2}$ were sealed in glass capillaries for the magnetic measurements. The crystals were perfectly transparent, indicating that no hydrolysis occurred.

Magnetic measurements were performed using a Superconducting Quantum Interference Device (SQUID) magnetometer (Quantum Design MPMS-XL-5 with a 5 T (50 kG) magnet), with the magnetic field H parallel and perpendicular to the crystallographic c axis.

3 Results

The single-crystal magnetic susceptibility is shown for $H \parallel c$ and $H \perp c$ orientations in Fig. 1. Below 25 K it is highly anisotropic, and was fitted using the spin Hamiltonian

$$\mathcal{H} = J(\hat{S}_1 \cdot \hat{S}_2) + D \sum_{i=1,2} \left[\hat{S}_{z_i}^2 - \frac{1}{3}(S_i(S_i+1) \right] + \sum_{i=1,2} g_i \mu_B \hat{S}_i \cdot H \qquad (1)$$

with $J = -2.23$ K, $D = -0.215$ K, and $g = 2.00$. The exchange splitting is ferromagnetic with an $S = 5$ dimer ground state, separated by 11.2 K from the next higher $S = 4$ state. The single-ion axial anisotropy parameter D can be correlated with the zero-field-splitting (ZFS) parameter of the dimer ground state by $D_{S=5} = 4/9 \cdot D = -0.096$ K.[16]

Magnetization measurements with $H \perp c$ showed the expected behavior for the above Hamiltonian and parameters, see the inset of Fig. 2. The results of magnetization measurements with $H \parallel c$ (H_z) were unusual. Fig. 2 shows

1.8 K results obtained with two different sweeping rates Γ. They exhibit a peculiar butterfly-shaped hysteresis with no remnant magnetization at $H_z = 0$. Similar behavior has been observed in $\mathbf{Mn_{12}}$ at 3.25 K, *i.e.* just above the blocking temperature.[17] The breadth of the wings increases with decreasing temperature and with increasing Γ. This is direct evidence for a slow relaxation process at 1.8 K. The effect is strongly T dependent, and we could observe it up to 5 K. For an infinitely slow Γ the butterfly hysteresis would disappear and the adiabatic curve (full line in Fig. 2) would be obtained. In order to quantitatively determine the relaxation dynamics, we performed magnetization relaxation experiments at fixed magnetic field H_z and temperature T, after saturation at 30 kG and subsequent quick reduction ($\Gamma \approx 150$ G/s) to the indicated H_z value. Typical decay curves are depicted in Fig. 3a for some selected values of H_z and T. The relaxation depends on both. At 1.8 K and $H_z = 3.3$ kG the relaxation is so slow that the equilibrium magnetization has not been reached after 40 minutes. For $H_z = 0$ at 1.8 K, on the other hand, the decay is about 4 times faster. At all fields the relaxation rate increases with temperature, as shown for $T = 1.8$ K and 3.0 K at $H_z = 0$ in the lower panel of Fig. 3a. Relaxation times τ were obtained from single-exponential fits to the relaxation curves for various H_z and T values. The field dependence of τ at 1.8 K, shown in Fig. 3b, exhibits 3 distinctive dips at $H_z = 0$, 1.1, and 2.7 kG. The temperature dependence of τ for a given value of H_z was fitted with the Arrhenius law

$$\tau = \tau_0 \cdot exp(\Delta E/kT) \quad . \tag{2}$$

At $H_z = 0$ the obtained parameter values are $\tau_0 = 70$ s and $\Delta E = 2.2$ K, corresponding to $\tau = 238$ s at 1.8 K.

Fig. 4 shows magnetization data obtained as follows: After saturation at +30 kG the field was quickly ($\Gamma \approx 150$ G/s) reduced to the given H_z values, including negative ones. The magnetization was measured within 50 s after reaching H_z. During such a fast sweep from +30 kG to −2.5 kG, *e.g.*, the magnetization switches instantaneously from positive to negative saturation when crossing $H_z = 0$.

4 Analysis and Discussion

Except for the butterfly hysteresis, the low-temperature magnetization curves in Fig. 2 are perfectly reproduced with the parameter values derived from the DC magnetic susceptibility data in the temperature range 1.8 K – 300 K. Furthermore, the shortest Fe–Fe distances between neighboring dimers are at least 8 Å,[15] which makes interdimer interactions extremely inefficient. Therefore the observed slow relaxation and butterfly hysteresis must be a genuine property of the $[Fe_2F_9]^{3-}$ dimer.

Our interpretation is based on a comparison with the observed behavior of single-molecule magnets such as $\mathbf{Mn_{12}}$[1,3], as well as the formalism developed for their interpretation. The appropriate picture representing the ZFS of the $S = 5$ dimer ground state with the negative $D_{S=5}$ is shown in Fig. 5. The barrier height in Fig. 5 at $H_z = 0$ is $\Delta = (|D_{S=5}|)S^2 = 2.40$ K. This is slightly larger than the kinetic activation energy $\Delta E = 2.2$ K determined from the magnetization relaxation. This difference is small, an indication that, if tunneling processes do contribute to the relaxation at the lowest temperatures, this contribution is not a dominant one. In the C_{3h} dimer symmetry, the full anisotropy Hamiltonian includes the higher–order terms $B_4^0\hat{O}_4^0$, $B_6^0\hat{O}_6^0$, and

$B_6^6\hat{O}_6^6$.[18] The $B_6^6\hat{O}_6^6$ term mixes wavefunctions with $\Delta M_S = \pm 6$. This allows for resonant tunneling at $H_z = 0$ between the M_S levels $-3/+3$ and at applied fields when the $M_S = -2/+4$ and $-1/+5$ levels cross, leading to significantly lower values of τ at these fields and hence to dips in a τ vs H_z plot. Therefore the observed dips in Fig. 3b are direct evidence for tunneling processes in $\mathbf{Fe_2}$. The dips are located at $H_z = 0$, 1.1, and 2.7 kG instead of 0, 1.4, and 2.85 kG, respectively, calculated without the higher-order terms. This indicates nonzero values for the parameters B_4^0 and B_6^0. In $\mathbf{Fe_2}$, the drop of τ due to resonant tunneling compared to pure thermal relaxation at non-resonant fields is only about 25-75%, see Fig. 3b. In contrast, τ decreases by 1–2 orders of magnitude in $\mathbf{Mn_{12}}$ when resonant tunneling is possible.[3] This is in line with our conclusion from the kinetic energy barrier, that although they occur, quantum tunneling processes are not dominant in $\mathbf{Fe_2}$. Instead, the purely thermal relaxation is dominant at all temperatures and field values. This distinctly different behavior from other SMMs is due to the combination of two facts: i) the thermal barrier in $\mathbf{Fe_2}$ does not exceed the barrier for tunneling processes by more than a factor of 1.6; and ii) the tunneling is phonon assisted and thus slowed down by an extremely slow energy exchange between the spin system and the phonon bath. This latter effect will now be analyzed.

The prefactor $\tau_0 = 70$ s obtained from the Arrhenius analysis of the relaxation dynamics at $H_z = 0$ is unusually large, $7 - 11$ orders of magnitude larger than in $\mathbf{Mn_{12}}$[1–4] and other SMMs [5,6,8–13]. It is much larger than the timescale of ac magnetic susceptibility measurements, which are usually used to characterize and quantify the relaxation behavior in SMMs. Only due to this extremely high τ_0 value are we able to observe a slow relaxation phenomenon

below 5 K with a barrier height of only $\Delta = 2.40$ K. In the SMMs reported so far, for comparison, Δ ranges from 7.6 K in $[Mn_4O_3F(OAc)_3(dbm)_3]$[7] to 79 K in $(PPh_4)[Mn_{12}O_{12}(O_2CEt)_{16}(H_2O)_4]$[9]. As indicated in Fig. 5, the magnetization in $\mathbf{Fe_2}$ can relax both by thermal activation over the energy barrier (full arrows) and by tunneling between the $M_S = -3/+3$ levels (dashed arrows). Both mechanisms rely on an interaction between the spin system and the crystal lattice degrees of freedom, *i.e.* on spin-phonon coupling. In this process, energy quanta corresponding to the energy differences between adjacent spin levels are exchanged between the spin system and the phonon bath. The extremely large τ_0 in $\mathbf{Fe_2}$ results from an extreme inefficiency of these processes below 5 K, and this can be ascribed to the following two factors: a small spin-phonon coupling parameter g_0 and a small density of phonon states in resonance with the energy spacings in Fig. 5. Quantitatively, the rate constant of a $\Delta M_S = \pm 1$ transition induced by phonon absorption or emission can be expressed as:[19]

$$W_{M_S \pm 1, M_S} = \frac{g_0^2 S_{\pm 1}}{48\pi\rho v^5 \hbar^4} \frac{(\varepsilon_{M_S \pm 1} - \varepsilon_{M_S})^3}{e^{(\varepsilon_{M_S \pm 1} - \varepsilon_{M_S})/kT} - 1}, \tag{3}$$

where $S_{\pm 1} = (S \mp M_S)(S \pm M_{S+1})(2M_S \pm 1)^2$. The number of phonons involved in the process depends on their energy $(\varepsilon_{M_S \pm 1} - \varepsilon_{M_S})$ and the energy distribution of the density of states, expressed by the sound velocity v in eq. 3, the mass density $\rho = 1.36$ g/cm^3[15] and the Bose population factor $(e^{(\varepsilon_{M_S \pm 1} - \varepsilon_{M_S})/kT} - 1)$.[19] We note that $(\varepsilon_{M_S \pm 1} - \varepsilon_{M_S})$ is about 1 order of magnitude smaller in $\mathbf{Fe_2}$ than in $\mathbf{Mn_{12}}$ and other SMMs. In all the SMMs reported so far,[1–13] the clusters are relatively large in size and contain organic ligands such as acetate. This gives rise to a large number of vibrational and rotational low-energy internal modes, leading to a high density of states

in the energy range most relevant for spin-phonon coupling. This is in sharp contrast to **Fe$_2$**, in which the $[Fe_2F_9]^{3-}$ unit consists of atomic ligands with stiff Fe–F bonds, reflected in the absence of low-energy vibrational or rotational modes. Compared to the other SMMs, the stiffness of the $[Fe_2F_9]^{3-}$ unit results in a strongly increased average sound velocity v in the crystal. Thus in **Fe$_2$** the density of phonon states $\rho_{ph} \propto 1/v^3$[20] is extremely low in the relevant energy range. The magnitude of the spin-phonon coupling parameter g_0 is governed by the strengths of spin-orbit and electron-phonon (orbit-lattice) couplings.[21,22] The latter is expected to be smaller in **Fe$_2$** compared to other SMMs due to the great stiffness of the $[Fe_2F_9]^{3-}$ unit. As spin-orbit coupling - in terms of the ZFS parameter D_S for the ground spin state - is also smaller in **Fe$_2$** compared to other SMMs,[1–13] we can expect a smaller spin-phonon coupling constant g_0 in **Fe$_2$**. Thus the efficiency of spin-phonon coupling is greatly reduced in **Fe$_2$** compared to other SMMs, and the smaller $(\varepsilon_{M_S\pm1} - \varepsilon_{M_S})^3$, the larger v^5, and the smaller g_0^2 factors all contribute to the drastic reduction of the transition rate constant W in **Fe$_2$**. As a consequence, the prefactor τ_0 in the Arrhenius expression is increased by 7–11 orders of magnitude.

The magnetization data shown in Fig. 4 obtained with $\Gamma \approx 150$ G/s exhibit a very fast reversal of the magnetization around $H_z = 0$. We ascribe this to a so-called phonon avalanche,[20] arising from a resonance of phonon absorption on one side of the barrier with phonon emission on the other side. A similar phenomenon has been observed in **Mn$_{12}$** at $H_z \neq 0$, induced by heat pulses[17] or extremely high sweeping rates.[23] The butterfly shape of the hysteresis in **Fe$_2$** is very similar to that reported for $K_6[V_{15}As_6O_{42}(H_2O)] \cdot 8H_2O$,[24] but in the latter system it has been attributed to a phonon bottleneck arising from dissipative spin reversal in the absence of an energy barrier. Our results show

that a butterfly-shaped hysteresis can also occur in the presence of a barrier.

Due to the phonon avalanche in **Fe$_2$**, the *reversal* of the magnetization at $H_z = 0$ is a much faster process than its *relaxation* to equilibrium. The smaller the sweeping rate Γ in the magnetization experiment, the closer is the system to equilibrium, as is nicely demonstrated by the decrease of the butterfly hysteresis with Γ in Fig. 2. After a fast ($\Gamma \approx 150$ G/s) reduction of H_z to 0, the system is therefore still out of equilibrium at the beginning of the relaxation measurement. Since its reversal is so fast, the magnetization then overshoots, i.e. it becomes slightly negative, before it relaxes to its adiabatic value. Therefore there is an observable negative magnetization relaxation at $H_z = 0$, see Fig. 3a, despite the fact that the butterfly hysteresis passes through the origin of the coordinates in Fig. 2.

In conclusion, we have shown **Fe$_2$** to exhibit unusually slow magnetization relaxation effects below 5 K. These can be ascribed to an energy barrier $\Delta = 2.40$ K resulting from the $S = 5$ dimer ground state of $[Fe_2F_9]^{3-}$ and a negative axial anisotropy. The relaxation partly occurs via a thermally-assisted quantum tunneling process. Compared to other SMMs, the energy exchange between the spin system and the phonons is extremely inefficient in **Fe$_2$**. Therefore the SMM phenomenon is observed at temperatures comparable to the barrier height and far above the blocking temperature, which for **Fe$_2$** is expected to lie in the mK regime. To our knowledge the **Fe$_2$** dimer is the smallest spin cluster so far to exhibit slow relaxation.

Acknowledgement. This work has been supported by the Swiss National Science Foundation and by the TMR program Molnanomag of the EU (HPRN-CT-1999-00012).

References

[1] A. Caneschi, D. Gatteschi, R. Sessoli, A.–L. Barra, L. C. Brunel, and M. Guillot, J. Am. Chem. Soc. **113**, 5873 (1991).

[2] J. Villain, F. Hartman–Boutron, R. Sessoli, A. Rettori,Europhys. Lett. **27**, 159 (1994).

[3] L. Thomas, F. Lionti, R. Ballou, D. Gatteschi, R. Sessoli, B. Barbara, Nature **12**, 145 (1996).

[4] J. R. Friedman, M. P. Sarachik, J. Tejada, R. Ziolo, Phys. Rev. Lett. **76**, 3830 (1996).

[5] C. Sangregorio, T. Ohm, C. Paulsen, R. Sessoli, D. Gatteschi, Phys. Rev. Lett **78**, 4645 (1997).

[6] S. M. J. Aubin, N. R. Dilley, L. Pardi, J. Krzystek, M. W. Wemple, L.-C. Brunel, M. Brian Maple, G. Christou, D. N. Hendrickson, J. Am. Chem. Soc. **120**, 4991 (1998).

[7] H. P. Andres, R. Basler, H. U. Güdel, G. Aromi, G. Christou, H. Büttner, B. Rufflé, J. Am. Chem. Soc. **122**, 12469 (2000).

[8] S. M. L. Aubin, M. W. Wemple, D. M. Adams, H.–L. Tsai, G. Christou, D. N. Hendrickson, J. Am. Chem. Soc. **118**, 7746 (1996).

[9] S. M. J. Aubin, Z. Sun, L. Pardi, J. Krzystek, K. Folting, L.–C. Brunel, A. Rheingold, G. Christou, D. N. Hendrickson, Inorg. Chem. **38**, 5329 (1999).

[10] J. Yoo, E. K. Brechin, A. Yamaguchi, M. Nakano, J. C. Huffman, A. L. Maniero, L.–C. Brunel, K. Awaga, H. Ishimoto, G. Christou, D. N. Hendrickson, Inorg. Chem. **39**, 3615 (2000).

[11] S. M. J. Aubin, Z. Sun, H. J. Eppley, E. M. Rumberger, I. A. Guzei, K. Folting, P. K. Gantzel, A. L. Rheingold, G. Christou, D. N. Hendrickson, Inorg. Chem. **40**, 2127 (2001).

[12] S. L. Castro, Z. Sun, C. M. Grant, J. C. Bollinger, D. N. Hendrickson, G. Christou, J. Am. Chem. Soc. **120**, 2365 (1998).

[13] A.–L. Barra, A. Caneschi, A. Cornia, F. Fabrizi de Biani, D. Gatteschi, C. Sangregoria, R. Sessoli, L. Sorace, J. Am. Chem. Soc. **121**, 5302 (1999).

[14] R. Schenker, H. Weihe, H. U. Güdel, Inorg. Chem. **40**, 4319 (2001).

[15] K. W. Krämer, R. Schenker, J. Hauser, H. Weihe, H. U. Güdel, H.-B. Bürgi, Z. Anorg. Allg. Chem. **627**, 2511 (2001).

[16] O. Kahn, *Molecular Magnetism*; VCH Publishers: New York, 1993, 142.

[17] C. Paulsen, J.–G. Park, B. Barbara, R. Sessoli, A. Caneschi, J. Magn. Magn. Mater. **140**, 1891 (1995).

[18] A. Abragam, B. Bleaney, *Electron Paramagnetic Resonance of Transition Metal Ions*; Clarendon Press: Oxford, 1970, 338.

[19] M. N. Leuenberger, D. Loss, Phys. Rev. B **61**, 1286 (2000).

[20] A. Abragam, B. Bleaney, *Electron Paramagnetic Resonance of Transition Metal Ions*; Clarendon Press: Oxford, 1970, 574.

[21] J. H. Van Vleck, Phys. Rev. **57**, 426 (1940).

[22] R. D. Mattuck, M. W. P. Strandberg, Phys. Rev. *119*, 1204 (1960).

[23] E. del Barco, J. M. Hernandez, M. Sales, J. Tejada, H. Rakoto, J. M. Broto, E. M. Chudnovsky, Phys. Rev. B **60**, 11898 (1999).

[24] I. Chiorescu, W. Wernsdorfer, A. Müller, H. Bögge, B. Barbara, Phys. Rev. Lett. **84**, 3454(2000).

Figure Captions

Fig. 1 Temperature dependence of the magnetic susceptibility χT of a single crystal of $(Et_4N)_3Fe_2F_9$ in the range 1.8–50 K (circles). The crystal was oriented with its c axis parallel ($H \parallel c$) and perpendicular ($H \perp c$) to the magnetic field of 1 kG. The solid lines are calculated using eq. 1 with the parameters $J = -2.23$ K, $D = -0.215$ K, and $g = 2.00$. The inset shows the $[Fe_2F_9]^{3-}$ dimer molecule and the magnetic field direction for both $H \parallel c$ and $H \perp c$ orientations.

Fig. 2 Positive wings of the butterfly hystereses of the magnetization in $H \parallel c$ orientation at 1.8 K for sweeping rates of $\Gamma \approx 3$ G/s ($*$) and $\Gamma \approx 1$ G/s ($\circ$). The 1.8 K magnetization in $H \perp c$ is shown in the inset. The solid lines are the adiabatic curves, calculated with $J = -2.23$ K, $D = -0.215$ K, and $g = 2.00$ derived from susceptibility measurements.

Fig. 3 a) Relaxation of the magnetization at fixed H_z and T as indicated, after saturation at 30 kG and quick ($\Gamma \approx 150$ G/s) sweep of the field to the indicated H_z value. The solid lines are fits to a single exponential law. Note the different scale for the $H_z = 0$ measurements. b) Dependence of the relaxation time τ from $H_z = 0$ with errors (3σ). The dotted line is a guide to the eyes.

Fig. 4 Magnetization data for $H \parallel c$ orientation at 1.8 K obtained as follows: After saturation at +30 kG, the field was quickly ($\Gamma \approx 150$ G/s) reduced to the given H_z values including negative ones, and the magnetization was measured within 50 s after reaching H_z. The solid line is the calculated adiabatic magnetization curve at 1.8 K, see also Fig. 2.

Fig. 5 Schematic plot of the potential energy *vs* magnetization direction for a $S = 5$ ground state split by a negative axial zero–field splitting at $H_z = 0$. The potential energy barrier is $\Delta = (|D_{S=5}|)S^2 = 2.40$ K. The full and broken arrows denote the thermal relaxation and possible tunneling pathways, respectively.

Figures

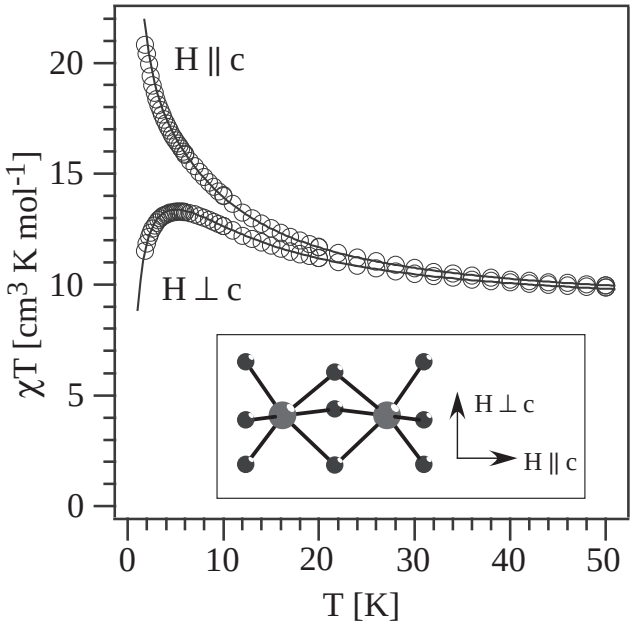

Fig. 1.

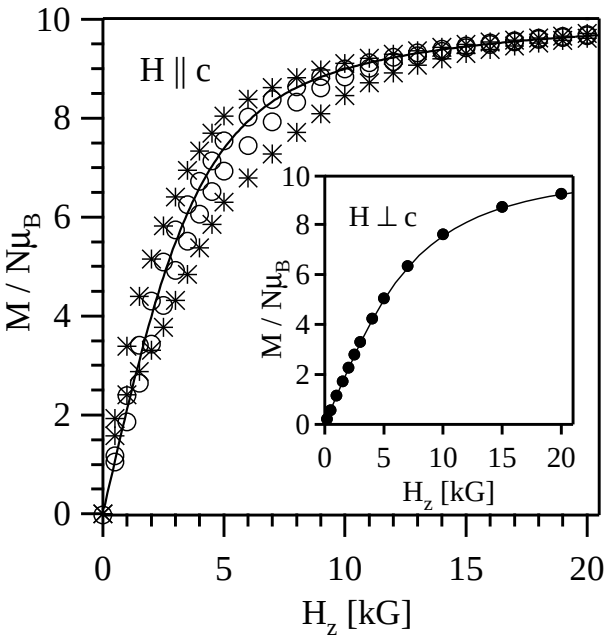

Fig. 2.

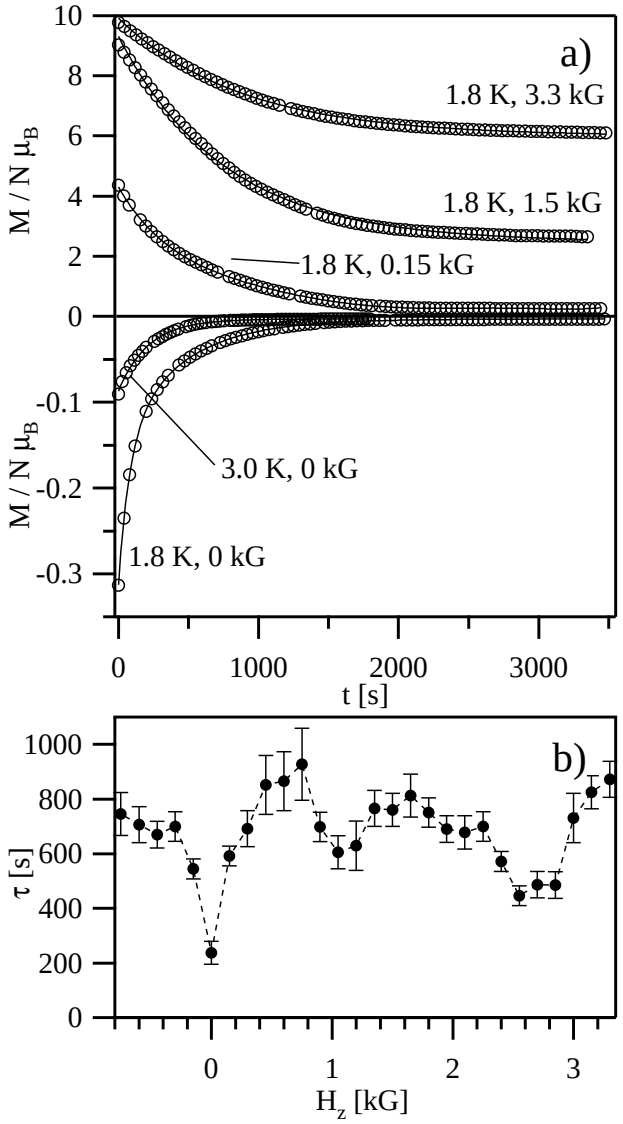

Fig. 3.

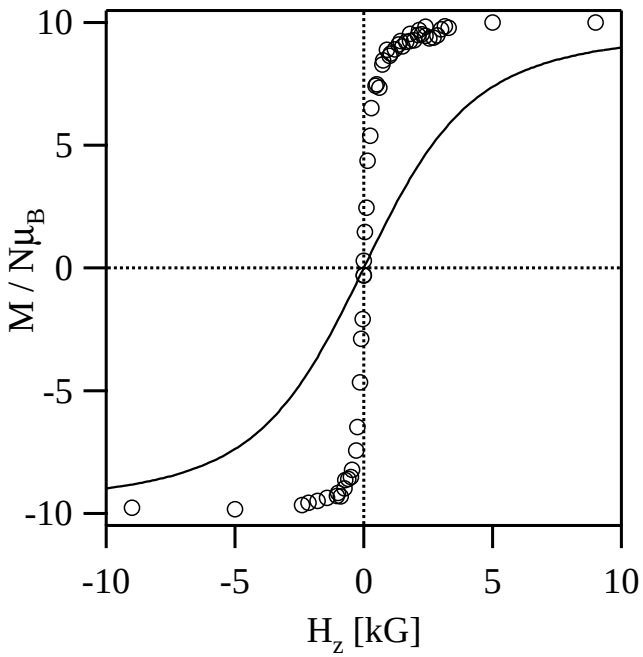

Fig. 4.

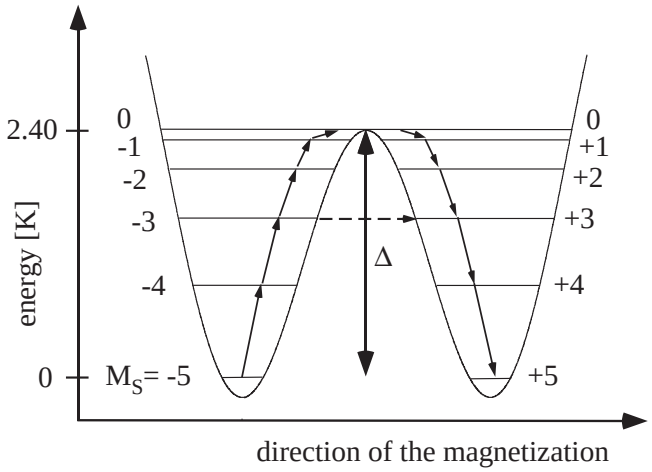
2.40
0
energy [K]
0
-1
-2
-3
-4
M_S= -5
Δ
0
+1
+2
+3
+4
+5
direction of the magnetization

Fig. 5.